J. Appl. Comput. Mech., 4(2) (2018) 125-132
DOI: 10.22055/JACM.2017.22700.1139

ISSN: 2383-4536
jacm.scu.ac.ir

Shahid Chamran University of Ahvaz

Journal of Applied and Computational Mechanics

Research Article

Finite Element Solutions of Cantilever and Fixed Actuator Beams Using Augmented Lagrangian Methods

Dongming Wei[1], Xuefeng Li[2]

[1] Department of Mathematics, School of Science and Technology, Nazarbayev University, Astana, 010000, Kazakhstan
[2] Department of Mathematics and Computer Science, Loyola University, New Orleans, LA 70118, USA

Received July 08 2017; Revised August 28 2017; Accepted for publication September 01 2017.
Corresponding author: Xuefeng Li, Li@Loyno.edu

Abstract. In this paper we develop a numerical procedure using finite element and augmented Lagrangian methods that simulates electro-mechanical pull-in states of both cantilever and fixed beams in microelectromechanical systems (MEMS) switches. We devise the augmented Lagrangian methods for the well-known Euler-Bernoulli beam equation which also takes into consideration of the fringing effect of electric field to allow a smooth transition of the electric field between center of a beam and edges of the beam. The numerical results obtained by the procedure are tabulated and compared with some existing results for beams in MEMS switches in literature. This procedure produces stable and accurate numerical results for simulation of these MEMS beams and can be a useful and efficient alternative for design and determining onset of pull-in for such devices.

Keywords: Microelectromechanical switch, Pull-in, Microbeam, Finite element solutions, Augmented Lagrangian methods.

1. Introduction

It is well-known that the beam-shaped microelectromechanical systems (MEMS) switches have many important applications, see, e.g., [1]. Sensors used in measuring blood pressure gradients in-vivo, in controlled micro robotic joints, in inkjet printers and in optical scanners are some examples of applications of such kind of switches, see e.g., [2] and [3] and the references therein. It is well known that the microbeams are susceptible to an instability known as pull-in. When the applied voltage is increased beyond a critical value, which is called the pull-in voltage, stable equilibrium positions of the microbeam cease to exist. This kind of instability greatly limits the range of stable operation of microbeams, see e.g., [4] and [5]. It is highly desirable to delay the onset of pull-in for better performance of the beams. The pull-in voltage depends on factors including the structural stiffness and the geometry of the microbeam and the residual stress etc. For a survey of such pull-in stability analysis of various MEMS devices, see, e.g., [6]. Researchers have also investigated the MEMS pull-in phenomenon using methods such as the penalty method [7], the normal flow algorithm [8], and the finite element methods [9, 10, 11]. More recently, see [12], in which finite element procedures based on commercial codes are presented for similar problems.
It is the goal of this work to provide a useful and efficient alternative procedure for numerical simulations of the beam devices studied in [4] and [5]. For completeness, we present the mathematical model considered in these two papers in the following. We begin with Table 1, listing the mechanical properties and the geometric quantities involved in the modelling and then we state the mathematical problems.

Published Online: January 05 2018

Table 1. Definitions of symbols.

Symbol	Definition
$\hat{E}$	effective modulus in [Pa]= $\begin{cases} E/(1-\nu^2), & \text{if } w \geq 5t \quad \text{(wide beams)} \\ E, & \text{if } w \geq 5t \quad \text{(narrow beams)} \end{cases}$
I	moment of inertia of cross-section of rectangular microbeam where origin of coordinates is the centroid of the cross-section A. $I = \int_A \lvert y \rvert^2 dydz = \frac{2w}{3}\left(\frac{t}{2}\right)^3 \left[m^4\right]$
v	deflection of the rectangular microbeam switch in [m], range= [0; g]
x	independent variable indicating beam location, range= [0; L]
T_a	axial force in microbeam = $\sigma wt\left[N\right]$
T_r	residual force of fixed-fixed microbeam= $\hat{\sigma} wt\left[N\right]$
ε_0	vacuum permittivity in [F/m]
w	width of microbeam in [m]
U	voltage applied to the microbeam switch in [V]
g	initial gap between the microbeam and the center conductor in [m]
$[0, L]$	endpoints of the microbeam, L is the length of microbeam in [m]
E	Young's modulus in [Pa]
ν	Poisson's ratio
t	thickness of microbeam in [m]
σ	axial stress in [Pa]
$\hat{\sigma}$	residual stress= $\sigma_r(1-\nu)$ [Pa], equals zero for cantilever beam
ΔL	beam elongation/compression in [m] due to axial stress $\approx \pm\frac{1}{2}\int_0^L \left(\frac{dv}{dx}\right)^2 dx$
σ_r	biaxial residual stress in [Pa]

Sadeghian, et al. [5] used a generalized differential quadrature method (GDQM) for the numerical simulations of microbeams governed by the Euler-Bernoulli beam equation:

$$(\hat{E}Iv'')'' - (T_t + T_a)v'' = \frac{\varepsilon_0 wU^2}{2(g - v(x))^2}, 0 \leq x \leq L, \tag{1}$$

Where $T_a = \sigma wt \approx (\hat{E}wt/(2L))\int_0^L \lvert v' \rvert^2 dx$. The boundary conditions considered are:

$$v(0) = 0, v'(0) = 0, v''(L) = 0, v'''(L) = 0 \tag{2}$$

For fixed-free cantilever beams, and

$$v(0) = 0, v'(0) = 0, v(L) = 0, v'(L) = 0 \tag{3}$$

For fixed-fixed beams. The above boundary value problems are considered by many as standard models for simulation of the microbeams in MEMS switches made of elastic materials. We adopt the standard notations and symbols appeared in the mathematical terms throughout this paper and list them in Table 1 with their definitions and explanations.

Zhang and Zhao [3], Sadeghian, et al. [5], and Ghazavi, et al. [11] also considered the socalled *Fringing effect of electric field* to allow a smooth transition of the electric field between center of a beam and edges of the beam. That effectively changes Eq. (1) into:

$$\begin{aligned} &(\hat{E}Iv'')'' - (T_r + T_a)v'' = \frac{\varepsilon_0 wU^2(1+f_f)}{2(g - v(x))^2} \equiv \tilde{f}(v), \\ &f_f = 0.65(g - v(x))/w, 0 \leq x \leq L. \end{aligned} \tag{4}$$

According to the pioneering work by Ghoussoub and Guo [13], the pull-in voltage for a microbeam described by Eq. (4) may be defined as a finite value U^* such that:

1. if $0 \leq U \leq U^*$ there exists at least one solution for Eq. (4);
2. If $U > U^*$, there is no solution for Eq. (4).

Due to nonlinearity involved in coefficient T_a and in function $\tilde{f}(v)$ for Eq. (4), we'll estimate the pull-in voltage U^* using the augmented Lagrangian methods introduced in this paper. We will use augmented Lagrangian methods with Hermite cubic finite element for Euler beams to simulate the pull-in deflections by solving Eq. (4) with the two standard boundary conditions stated in Eqs. (2) and (3), respectively. The algorithm and the code developed based on these methods can provide maximum deflections and maximum stresses which are important data for designing stronger and more reliable devices of this type. The pull-in simulations of both cantilever and fixed–fixed beam MEMS switches have been implemented by using the

data investigated by Hu, et al. [2], and by Sadeghian, et al. [5]. These results obtained from the simulations are expected to be useful in the optimum design of MEMS switches or other actuators. Because the three terms in Eq. (4) are quantities of different magnitudes, it is necessary to non-dimensionalize the equation before we begin numerical computations of its approximate solutions.

2. Formulation of Augmented Lagrangian Methods for Microbeams

We'll convert the problem in Eq. (4) into an appropriate Lagrangian in this section.

2.1 Non-dimensionalization of the Euler-Bernoulli Beam Equation

Since v is the deflection of the microbeam from the stationary position that is expected to have a range in [0; g], and x is the coordinate in domain [0; L], we may non-dimensionalize Eq. (4) by introducing the following variables.

$$\xi = \frac{x}{L} \leftrightarrow x = L\xi, and \zeta(\xi) = \frac{v(x)}{g} \leftrightarrow v(x) = g\zeta(\xi). \tag{5}$$

By definition, $\zeta \in [0, 1]$ and $\xi \in [0, 1]$ are both dimensionless. As a result, the non-dimensionalized Euler-Bernoulli beam equation becomes:

$$(\zeta'')'' - \alpha_1(\zeta')\zeta'' = \beta_3 f(\zeta), \ 0<\xi<1, \tag{6}$$

where

$$f(\zeta) = \frac{2g^2}{\varepsilon_0 w U^2}\tilde{f}(v) = \frac{1+f_f}{(1-\zeta(\xi))^2}, \tag{7}$$

$$f_f = 0.65\left[\frac{g-v(x)}{w}\right] = \frac{0.65g}{w}(1-\zeta), \tag{8}$$

$$\alpha_1(y) = \frac{(T_r+T_a)L^2}{\hat{E}I} = \frac{T_r L^2}{\hat{E}I} + \frac{T_a L^2}{\hat{E}I} = \frac{T_r L^2}{\hat{E}I} + \frac{wtg^2}{2I}\int_0^1 |y|^2 d\xi, \tag{9}$$

$$\beta_3 = \frac{\varepsilon_0 w U^2 L^4}{2\hat{E}Ig^3}. \tag{10}$$

The boundary conditions in Eqs. (2) And (3) become:

$$\zeta(0) = 0, \zeta'(0) = 0 (\text{plus } \zeta(1) = 0, \zeta'(1) = 0 \quad \text{for fixed-fixed beams}) \tag{11}$$

2.2 The Associated Minimization Functional

With standard manipulations, we can derive a minimization problem whose stationary point corresponds to a solution to the non-dimensionalized Euler–Bernoulli beam Eq. (6).

$$\text{Minimize } I(\zeta) = \int_0^1 \frac{1}{2}|\zeta''|^2 d\xi + \beta_1\int_0^1 |\zeta'|^2 d\xi + \beta_2\left(\int_0^1 |\zeta'|^2 d\xi\right)^2 - \int_0^1 \beta_3 F(\zeta) d\xi, \tag{12}$$

where

$$\beta_1 = \frac{T_r L^2}{2\hat{E}I}, \tag{13}$$

$$\beta_2 = \frac{wtg^2}{8I}, \tag{14}$$

subject to boundary conditions (11). Here, $F(\zeta)$ is defined in Eq. (15).

$$\begin{aligned} &\frac{dF(\zeta)}{d\zeta} = F'(\zeta) = f(\zeta), \\ &F(\zeta) = \int f(\zeta) d\zeta = \int \frac{1+f_f}{(1-\zeta(\xi))^2} d\zeta \\ &= \int \frac{1+\frac{0.65g}{w}(1-\zeta)}{(1-\zeta(\xi))^2} d\zeta = \frac{1}{1-\zeta} - \frac{0.65g}{w} ln(1-\zeta). \end{aligned} \tag{15}$$

Parameter α_1 (y) as defined in Eq. (9) can also be expressed in terms of β_1 and β_2:

$$\alpha_1(y) = 2\beta_1 + 4\beta_2 \int_0^1 |y|^2 d\xi. \tag{16}$$

Notice that β_1 (through T_r) is the coefficient for a term associated with longitudinal forces on the beam. We can model cantilever beams using the minimization problem (12) by assuming that β_1 is zero.

2.3 Formulating the Associated Lagrangians

Straightly based on algorithms proposed by Fortin and Glowinski [14], we can develop a Lagrangian shown in Eq. (17) that is associated with the minimization functional (12).

$$\begin{aligned} \ell(\zeta, p, q, \theta, \lambda) &= \int_0^1 \frac{1}{2}|q|^2 d\xi + \beta_1 \int_0^1 |p|^2 d\xi + \beta_2 \left(\int_0^1 |p|^2 d\xi \right)^2 - \int_0^1 \beta_3 F(\zeta) d\xi \\ &+ \int_0^1 \theta(\zeta' - p) d\xi + \int_0^1 \lambda(\zeta'' - q) d\xi. \end{aligned} \tag{17}$$

Here, p and q are supplementary variables that are linked to ζ by the linear equality relations

$$p - \zeta' = 0, q - \zeta'' = 0, \tag{18}$$

And θ, λ are Lagrangian multipliers. An associated augmented Lagrangian of (17) is

$$L_{r,s}(\zeta, p, q, \theta, \lambda) = \ell(\zeta, p, q, \theta, \lambda) + \frac{r}{2} \int_0^1 (\zeta' - p)^2 d\xi + \frac{s}{2} \int_0^1 (\zeta'' - q)^2 d\xi, \tag{19}$$

Where $r > 0$ and $s > 0$ are two pre-chosen constants. We require that

$$\zeta \in H^2(0,1), p \in H^0(0,1), q \in H^0(0,1), \theta, \lambda \in H^0(0,1), \tag{20}$$

In order for Lagrangian (17) and the augmented Lagrangian (19) to exist, along with the appropriate boundary condition requirements. Here, $H^0(0, 1)$, $H^1(0, 1)$, and $H^2(0, 1)$ are Sobolev (Hilbert) spaces [14] consist of square–integrable functions over [0; 1] having 0-th, 1st and 2nd weak derivatives that are also square–integrable over [0; 1] , respectively. With simple manipulations, we can show that a saddle point of augmented Lagrangian (19) corresponds to a weak solution to Eq. (6). For brevity, we omit the derivation here. However, requirement (20) is too demanding on ζ for numerical simulations. A slightly different Lagrangian with a weaker requirement on ζ is proposed next. Alternatively, based on algorithms proposed by Fortin and Glowinski [14], we can also develop a Lagrangian shown in Eq. (21) that is associated with the minimization functional (12).

$$\begin{aligned} \ell(\zeta, p, q, \theta, \lambda) &= \int_0^1 \frac{1}{2}|q|^2 d\xi + \beta_1 \int_0^1 |p|^2 d\xi + \beta_2 \left(\int_0^1 |p|^2 d\xi \right)^2 - \int_0^1 \beta_3 F(\zeta) d\xi \\ &+ \int_0^1 \theta(\zeta' - p) d\xi + \int_0^1 \lambda(p - q) d\xi. \end{aligned} \tag{21}$$

Here, p and q are supplementary variables that are linked to ζ by the linear equality relations

$$p - \zeta' = 0, q - p' = 0, \tag{22}$$

And θ, λ are Lagrangian multipliers. An associated augmented Lagrangian of (21) is:

$$L_{r,s}(\zeta, p, q, \theta, \lambda) = \ell(\zeta, p, q, \theta, \lambda) + \frac{r}{2} \int_0^1 (\zeta' - p)^2 d\xi + \frac{s}{2} \int_0^1 (p' - q)^2 d\xi, \tag{23}$$

where $r > 0$ and $s > 0$ are two pre-chosen constants. We require that

$$\zeta \in H^1(0,1), p \in H^1(0,1), q \in H^0(0,1), \theta, \lambda \in H^0(0,1), \tag{24}$$

Table 2. Boundary conditions for augmented Lagrangian

	ζ	p	q
Cantilever beams	$\zeta(0)=0$, $\zeta'(0)=0$	$p(0)=0$	None
Fixed-fixed	$\zeta(0)=0$, $\zeta'(0)=0$	$p(0)=0$	None
beams	$\zeta(1)=0$, $\zeta'(1)=0$	$p(1)=0$	None

in order for Lagrangian (21) and the augmented Lagrangian (23) to exist. We also enforce boundary conditions as listed in Eq. (11), summarized in Table 2. With simple manipulations, we can again show that a saddle point of augmented Lagrangian (23) corresponds to a weak solution to Eq. (6). For brevity, we omit the derivation here. Notice that requirement (24) is weaker on ζ than in requirement (20). Augmented Lagrangian (23) is therefore preferred over augmented Lagrangian (19) for the purpose of numerical simulations.

Table 3. ALG1: Finding a saddle point of augmented Lagrangian (23).

1. Choose arbitrary initial guess $\theta(0)$ and $\lambda(0)$.
2. For k ≥ 0, calculate $(\zeta^{(k)}, p^{(k)}, q^{(k)}) \in V$, by

$$L^{(1)}{}_{r,s}(\zeta^{(k)}, p^{(k)}, q^{(k)}, \theta^{(k)}, \lambda^{(k)}) = \min_{(\zeta,p,q)\in V} L^{(1)}{}_{r,s}(\zeta, p, q, \theta^{(k)}, \lambda^{(k)}), \tag{25}$$

subject to boundary conditions in Table 2, where $V = H^1(0,1)\times H^1(0,1)\times H^0(0,1)$, and calculate $\theta^{(k+1)}, \lambda^{(k+1)} \in H^0(0,1)$ by

$$\theta^{(k+1)} = \theta^{(k)} + \rho_1((\zeta^{(k)})' - q^{(k)}), \lambda^{(k+1)} = \lambda^{(k)} + \rho_2((p^{(k)})' - q^{(k)}), \tag{26}$$

Where ρ_1 and ρ_2 are two pre-chosen positive constants.

3. Check for convergence. Repeat the above procedure when needed. Convergence is reached when the following conditions are met

$$\begin{cases} \left\|\zeta^{(k+1)} - \zeta^{(k)}\right\| \le \varepsilon_r \left\|\zeta^{(k)}\right\|, \\ \left\|p^{(k+1)} - p^{(k)}\right\| \le \varepsilon_r \left\|p^{(k)}\right\|, \left\|q^{(k+1)} - q^{(k)}\right\| \le \varepsilon_r \left\|q^{(k)}\right\|, \end{cases} \tag{27}$$

For a pre-chosen relative tolerance ε_r.

In Table 3, we introduce the algorithm that finds a saddle point of augmented Lagrangian (23), based on the algorithm proposed by Fortin and Glowinski [14] (page 108, ALG1). Fortin and Glowinski [14] (page 110, ALG2) further propose to use another iteration (inner iteration) to find the stationary point in Eq. (25), as shown in Table 4. A computational flow chart that illustrates the augmented Lagrangian methods applied to Eq. (6) is shown in Fig. 1. It is possible but highly unlikely that one would be able to solve for $\zeta^{(k,m)}$, $p^{(k,m)}$ and $q^{(k,m)}$ exactly from Eqs. (28) and (29), respectively. In practice, we use the standard finite element methods with cubic Hermite shape functions to find approximate solutions to $\zeta^{(k.m)}$, $p^{(k.m)}$ and $q^{(k,m)}$. Details of finite element approximations are therefore omitted here.

Table 4. ALG2: Finding $\zeta^{(k)}, p^{(k)}$ and $q^{(k)}$ with an inner iteration.

1. For a fixed k, $p^{(k,0)} = p^{(k-1)}, q^{(k,0)} = q^{(k-1)}$.
2. For $m \ge 1$,

$(a) \forall \eta \in H^1(0,1)$ that satisfies ζ boundary conditions in Table 2, solve Eq. (28) for $\zeta^{(k,m)}(\xi)$,

$$\lim_{t\to 0} \frac{\partial}{\partial t} L^{(1)}{}_{r,s}(\zeta^{(k.m)}(\xi) + t\eta, p^{(k,m-1)}, q^{(k,m-1)}, \theta^{(k)}, \lambda^{(k)}) = 0, \tag{28}$$

subject to boundary conditions in Table 2.

(b) Using $\zeta^{(k.m)}(\xi)$ calculated in the previous step, $\forall \eta_1 \in H^1(0,1)$ that satisfies p-boundary conditions in Table 2, and $\forall \eta_2 \in H^0(0,1)$ that satisfies q-boundary conditions in Table 2, solve system of Eq. (29) for $p^{(k,m)}(\xi)$ and $q^{(k,m)}(\xi)$,

$$\lim_{\alpha,\beta\to 0} \frac{\partial}{\partial(\alpha,\beta)} L^{(1)}{}_{r,s}(\zeta^{(k.m)}(\xi), p^{(k,m)} + \alpha\eta_1, q^{(k,m)} + \beta\eta_2, \theta^{(k)}, \lambda^{(k)}) = 0, \tag{29}$$

subject to boundary conditions in Table 2.

3. Repeat for a certain number of times, or until convergence. Then

$$\zeta^{(k)} = \lim_{m\ge 1} \zeta^{(k.m)}, p^{(k,m)} = \lim_{m\ge 1} p^{(k.m)}, q^{(k)} = \lim_{m\ge 1} q^{(k.m)}. \tag{30}$$

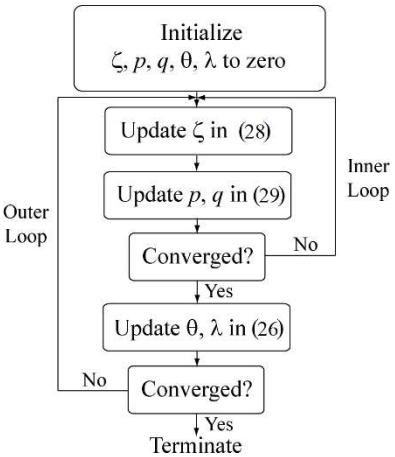

Fig. 1. Computational flow chart of augmented Lagrangian methods.

3. Further Discussions

In the previous section, we've demonstrated that the augmented Lagrangian methods may be used to formulate a numerical algorithm that finds approximate solutions to the Euler-Bernoulli beam equation. The new approach takes advantage of a reformulation of the Euler-Bernoulli beam equation into an optimization problem. It then applies the augmented Lagrangian methods that introduce additional variables in place of derivatives of the deflection function u. As it is well-known, there are many more beam theories besides the Euler-Bernoulli theory. One of the widely used beam theory is the Timoshenko beam theory. Unlike the Euler-Bernoulli beam theory where only the effects of bending moment were considered, the Timoshenko beam theory takes into account shear deformation and rotational bending effects. See [15, 16] for introductions, and [17, 18, 19, 20, 21] for some of the more recent applications of the theory. As indicated by Fortin and Glowinski [14], the augmented Lagrangian methods may be applied to all kinds of optimization problems where the functionals involved are dependent of derivatives of the variable function(s). For Timoshenko beams, at least in the case of static Timoshenko beam equations [17, 21], the authors believe that the augmented Lagrangian methods may be helpful in providing a reliable and stable algorithm for finding numerical solutions to Timoshenko beam equations, since the beam equations can be reformulated as optimization problems too. We plan to investigate applications of the augmented Lagrangian methods to Timoshenko beam equations in our future studies.

4. Numerical Results

In the current section, we present numerical results obtained by applying augmented Lagrangian methods to solve the Euler-Bernoulli beam Eq. (6), subject to boundary conditions (11) using Lagrangian (23). The test problems are one case of cantilever beam studied by Hu, Chang and Huang [2], and one case of fixed-fixed beams studied by Sadeghian, Rezazadeh and Osterberg [5].

We list common geometric and material properties of the beams under study in Table 5. Our numerical results from augmented Lagrangian methods match with those from [2] and [5] very well, as shown in Tables 6 and 7.

Table 5. Geometric and material properties of beams.

Parameters	beam in [2]	beam in [5]
Width w	5mm	50 μm
Length L	20mm	250/350 μm
Thickness t	57μm	3 μm
Initial gap g	92μm	1 μm
Young's modulus E	155.8GPa	169 GPa

The vacuum permittivity is ε_0 = 8:854 pF/m for all beams. Poisson's ratio ν = 0.06 is used for the beam in [5] because the effect of residual stress is incorporated. Because of parameters ρ_1 and ρ_2 in ALG1 of Table 3, as well as parameters r and s in ALG2 of Table 4, the augmented Lagrangian methods are highly flexible.

Table 6. Numerical results for the cantilever beam by ALM.

Voltage (V)	End gap (μm) [2]	End gap (μm) by ALM	Relative error
$\rho_1 = \rho_2 = 0.00208, r = s = 458.0$			
20	90.50	90.29	-0.23%
40	84.60	84.56	-0.05%
60	70.00	71.04	1.48%
65	64.00	63.81	-0.30%
67	59.00	58.81	-0.32%
$\rho_1 = \rho_2 = 1.0, r = s = 615.0$			
20	90.50	90.24	-0.29%
40	84.60	84.34	-0.31%
60	70.00	70.54	-0.78%
65	64.00	63.44	-0.87%
67	59.00	59.01	0.02%

Table 7. Numerical results for fixed-fixed beams by ALM.

	Beam length L = 250 μm			Beam length L = 350 μm		
Stress(MPa)	Pull-in voltage [5]	Pull-in voltage by ALM	Relative error	Pull-in voltage [5]	Pull-in voltage by ALM	Relative error
0	40.10	39.80	-0.75%	20.30	20.15	-0.74%
100	57.60	57.50	-0.17%	35.80	35.70	-0.28%
-25	33.60	33.66	0.18%	13.70	13.68	-0.15%

In other words, there are "four degrees of freedom" that one can use to fine-tune algorithms ALG1 and ALG2 to produce

the best results possible. This is demonstrated in Table 6 where results from two different sets of parameters were calculated with different degrees of accuracy. Fortin and Glowinski have also given out recommendations on how parameters should be chosen in [14]. Generally speaking, an augmented Lagrangian method is an iterative method as shown in Table 3. However, it incorporates an inner iterative process as indicated in Table 4 as well as in Fig. 1. The number of inner iterations is a parameter to be chosen for each problem the method solves. Our numerical results have demonstrated that even though using one inner iteration may be acceptable in certain cases, using two inner iterations will improve results dramatically. Furthermore, using more than two inner iterations for each inner loop does not seem to affect much of the outcomes. See Table 8 for details.

5. Conclusion

An algorithm is developed based on the Augmented Lagrangian Methods for numerical simulation of the pull-in phenomenon in design of MEMS beam switches. The algorithm is implemented by using finite elements to create a computer code which is run successfully using some standard data and parameters in literature. It has provided stable and accurate solutions comparing with those in literature. This algorithm can be useful, stable, and efficient alternative for design and simulation of such devices.

Table 8. Effects of inner iterations of ALM.

Voltage (V)	Error with 1 iter.	Error with 2 iter.	Error with 5 iter.
20	-0.12%	-0.23%	-0.23%
40	0.50%	-0.05%	-0.05%
60	4.03%	1.48%	1.48%
65	4.59%	-0.30%	-0.30%
67	7.76%	-0.32%	-0.33%

Acknowledgments

The authors would like to express their deep appreciation to referees for their helpful comments. Their suggestions have made this manuscript a better publication.

References

[1] Younis, M. I., *MEMS Linear and nonlinear statics and dynamics*, Springer, 2011.
[2] Hu, Y. C., Chang, C. M., Huang, S. C., Some design considerations on the electrostatically actuated microstructures, *Sensors and Actuators A*, 112, 2004, pp. 155–161.
[3] Zhang, L. X., Zhao, Y. P., Electromechanical model of RF MEMS switches, *Microsystem Technologies*, 9(6-7), 2003, pp. 420-426.
[4] Batmanov, A., *Design, modeling and fabrication of radio-frequency microelectromechanical switches and coplanar filters*, Master's thesis, Otto-von-Guericke-Universitat Magdeburg, April, 2010.
[5] Sadeghian, H., Rezazadeh, G., Osterberg, P. M., Application of the generalized differential quadrature method to the study of pull-in phenomena of MEMS switches, Journal of Microelectromechanical Systems, 16(6), 2007, pp. 1334–1340.
[6] Zhang, W. M., Yan, H., Peng, Z. K., Meng, G., Electrostatic pull-in instability in MEMS/NEMS: A review, *Sensors and Actuators A*, 214, 2014, pp. 187–218.
[7] Joglekar, M. M., Pawaskar, D. N., Shape optimization of electrostatically actuated microbeams for extending static and dynamic operating ranges, *Structural and Multidisciplinary Optim*ization, 46, 2012, pp. 871–890.
[8] Abdalla, M. M., Reddy, C. K., Faris, Waleed F., Gurdal, Z., Optimal design of an electrostatically actuated microbeam for maximum pull-in voltage, *Computers and Structures*, 83, 2005, pp. 1320–1329.
[9] Abdelhakim, L., Numerical model for electro-mechanical analysis based on finite Element method, *PAMM: Proceedings in Applied Mathematics and Mechanics*, 13, 2013, pp. 245–246.
[10] Rochus, V., Rixen, D. J., Golinval, J. C., Finite element modeling of electro-mechanical coupling in capacitive micro-systems, *Nano Science and Technology Institute-Nanotech 2005*, 3, 2005, pp. 704-707.
[11] Ghazavi, M. R., Rezazadeh, G., Azizi, S., Finite element analysis of static and dynamic pullin instability of a fixed-fixed micro beam considering damping effects, *Sensors Transducers*, 103(4), 2009, pp. 132–143.
[12] Zhou, W., Shen, H., Guo, Z., Peng, B., Modeling the pull-in behavior of electrostatically actuated micro beams by an approximate finite element method, *International Journal of Numerical Modelling*, 27, 2014, pp. 89–98.
[13] Ghoussoub, N., Guo, Y. J., On the partial differential equations of electrostatic mems devices: stationary case, *SIAM Journal on Mathematical Analysis*, 38(5), 2007, pp. 1423–1449.
[14] Fortin, M., Glowinski, R., *Augmented Lagrangian methods: Applications to the numerical solution of boundary-value problems*, 1st Edition, North Holland, 1983.
[15] Timoshenko, S. P., *Strength of materials: part 1*, 2nd Ed. New York: Van Nostrand Company, 1940.
[16] Hjelmstad, K., *Fundamentals of Structural Mechanics*, Second edition, Chapter 7. Springer Inc., 2005.
[17] Antes, H., Fundamental solution and integral equations for Timoshenko beams, *Computers and Structures*, 81, 2003, pp. 383–396.
[18] Kahrobaiyan, M. H., Asghari, M., Ahmadian, M. T., Timoshenko beam element based on the modified couple stress theory, *International Journal of Mechanical Sciences*, 79, 2014, pp. 75–83.

[19] Zhang, B., He, Y. M, Liu, D. B., Gan, Z. P., Shen, L., Non-classical Timoshenko beam element based on the strain gradient elasticity theory, *Finite Elements in Analysis and Design*, 79, 2014, pp. 22–39.
[20] Talebi, S., Uosofvand, H., Ariaei, A., Vibration analysis of a rotating closed section composite Timoshenko beam by using differential transform method, *Journal of Applied and Computational Mechanics*, 1(4), 2015, pp. 181-186.
[21] Ai, Z. Y., Cai, J. B., Static interaction analysis between a Timoshenko beam and layered soils by analytical layer element/boundary element method coupling, *Applied Mathematical Modelling*, 40, 2016, pp. 9485–9499.